Nadher D. Radhy et al /J. Pharm. Sci. & Res. Vol. 11(2), 2019, 456-463

ISSN:0975-1459
Journal of Pharmaceutical Sciences and Research
www.jpsr.pharmainfo.in

Synthesis of Graphene Oxide/Hydrogel Composites and Their Ability for Efficient Adsorption of Crystal Violet

Nadher D. Radhy[1], Layth S. Jasim[2*]

[1] *Department of Chemistry Pharmaceutical, College of Pharmacy, University of Al-Qadisiyah, Iraq*
[2] *Department of Chemistry, College of Education, University of Al-Qadisiyah, Iraq*

Abstract

Composite hydrogels Graphite oxide (GO) /poly (acrylic acid – maleic acid) superabsorbent composites were containing different amounts of graphene oxide were synthesized by free radical polymerization of acrylic acid and maleic acid as a monomers, using N,N-methylenebisacrylamide as cross-linker and ammonium persulfate as initiator. The synthesized composites hydrogels were characterized by Fourier transform infrared spectroscopy (FTIR), field emission scanning electron microscopy (FE-SEM), and UV-vis spectroscopy. The synthesis composite hydrogels were used as adsorbents for removal of a cationic dye, crystal violet (CV) from aqueous solution. The isotherm of adsorption and the effect of different experimental conditions such as graphene oxide content, pH of the solution, contact time, ionic strength and initial dye concentration on adsorption capacity were then investigated. Parameters related to isotherm models were calculated and discussed. It was found that adsorption is well described by Langmuir isotherm models. The synthesized adsorbents showed high efficiency in removal of crystal violet and a very high adsorption capacity. No significant loss of removal efficiency was observed even after five cycles of adsorption.

Keywords: Graphene oxide, hydrogel composites, adsorption, crystal violet.

INTRODUCTION

Synthetics dyes have been widely used in textile, food, cosmetics, pharmaceutical industries and with microbiological purposes as well. With the development of technology and industry, more and more attention has been paid to dyes as water pollutants. The total dye production exceeds the 700,000 tons per year and about 2% of this production is discharged in the effluent from manufacturing operations [1]. There are commonly about 10–15% of unused dyestuff entering the wastewater directly in the staining process but the loss of some reactive dyes in the dyeing process could reach 50% [2]. One of the major problems that water coloration entails is the reduction of sunlight transmission, which affects photosynthesis and harms aquatic ecosystems [3]. In addition, many of the synthetic dyes are toxic and carcinogenic [4].

In the last years, several wastewater treatment methods have been developed. Some examples of those techniques are coagulation, chemical oxidations, and biological or enzymatic treatment. However, most of them are not capable of achieving high quality treated water or carry high implementation costs [5]. Depending on the adsorbent source, adsorption technologies represent one of the most efficient and cheap alternatives towards the treatment of wastewater, which may contain several kinds of pollutants, for instance, dyes. Other advantages of these decontamination methods are the facile scaling-up, high-efficiency sorption without releasing any co-product to the environment and the possibility of recovering the adsorbent once the treatment is finished in the case of liquid-solid adsorptions [6]. Several adsorbent materials have already shown the potential for dye adsorption [7, 8].

As a kind of novel polymer materials, polymer hydrogels have been widely applied in drug delivery systems, biosensors, sustained drug-release, and etc. [9-13]. However, its poor mechanical strength (toughness and crack resistance) greatly limited their applications [14-17]. In the past decade, many investigators have been devoted to improving the mechanical performance of the hydrogels. Added nanofillers (such as silica, carbon nanotubes) to the hydrogels is considered to be an effective way to enhance the mechanical strength of the hydrogels. For traditional hydrogel, three-dimensional (3D) network was usually formed by one-dimensional (1D) molecules aggregation (e.g. nanofibers and tubes). However, the framework of graphene-based hydrogels was different from traditional hydrogel since to the two-dimensional (2D) lattice structure of GO, and the various oxygen-containing groups (hydroxyl, epoxide groups and carboxyl groups etc.) on the basal planes and edges of modified graphene. Meanwhile, these oxygen-containing groups impart GO strong interaction with polar small molecules or polymers to form hydrogels. Therefore, the graphene composite hydrogel was always synthesized by the cross-linking of polymer chains driven by various kinds of non-covalent bonds (i.e., hydrogen bonding) [18-20].

In this article, GO/poly (acrylic acid-Maleic acid) P (AA-MA) composite hydrogel was prepared, in which the P (AA-MA) acted as the cross-linker and the main driven force was various noncovalent interactions. This work demonstrated that the GO/P (AA-MA) hydrogels exhibited excellent mechanical strength and rapid dye adsorption capability. It can be expected that GO/P (AA-MA) hydrogels with excellent mechanical properties could play a more important role in adsorption field.

MATERIALS AND METHODS

Chemicals and materials

Natural graphite powders, potassium permanganate ($KMnO_4$), sodium nitrate ($NaNO_3$), concentrated sulfuric acid, hydrochloric acid, hydrogen peroxide (30%), acrylic acid(AA), maleic acid (MA), N,N-methylene-bisacrylamide (MBA), ammonium persulfate (APS), crystal violet (CV) and Sodium hydroxide were purchased from Kemiou Chemical Reagent Co, Ltd, China. All the reagents used were analytical grade pure with no further purification, and all the solutions were prepared with deionized water.

Preparation of GO

GO was prepared according to modified Hummers, method [21]. Briefly, 1.0 g of sodium nitrate was stirred with 1.0 g of natural graphite in an ice-water bath for 10 minutes. Once the mixture was well mixed, 46 mL of sulfuric acid was added gradually into the mixture. The mixture was kept between the temperature range of 0℃ to 5℃ in the ice-water bath as a safety precaution. While maintaining vigorous agitation, 6.0g of potassium permanganate was added into the suspension gradually. The rate of addition was controlled to prevent the temperature of the mixture from exceeding 20 ℃. The mixture was kept mixing for a total of 2 hours with the temperature of the ice-water bath kept at ≤5℃. The ice-water bath was then removed and the mixture was stirred overnight at room temperature. As the reaction progressed, the mixture gradually thickened. After a night of stirring, the mixture became pasty and it became brownish grey in color. Thereafter, 135 mL of deionized water was slowly stirred into the paste and this resulted in violent effervescence and a temperature hike to 98℃. A watch glass was used to minimize evaporation and the level of the mixture was maintained at 250 mL with the periodical addition of deionized water for 1 hour. Subsequently, the heater was turned off and the mixture was then left to cool for 1 hour to room temperature. Once completed, 10 mL of hydrogen peroxide (30%) was added dropwise to reduce the residual permanganate and manganese dioxide to colorless soluble manganese sulfate. After the filtration of the mixture, the residue was washed with (10% HCl) solution four times and ultrapure water five times. The product was dialyzed with deionized water for one week. Then, it was dried at 60℃ and stored for further use. To prepare fully exfoliated GO nanosheets with different concentration (3-6 mg/mL), different amount of GO powder was dispersed into 100 mL deionized water, followed by an ultrasonic for 30 min to form a yellow-brown stable GO solution.

Preparation of GO/P(AA-MA) composite

For the preparation of GO/P(AA-MA) composite, firstly, 2 mL GO (3, 4, 5 and 6 mg/mL) water solution mixed with of AA(0.08 mol), MA(0.02 mol), MBA(0.032-0.22 mmol) APS(0.015g) were dissolved in double distilled water to total volume of 10 mL Then, the mixture was sonicated for 10 min and became homogenized were poured into a glass container, heated slowly to 55 ^{0}C (over about 10 min) under a N_2 atmosphere and kept at this temperature for 2 h . After being cooled down to room temperature, the resulting hydrogel was immersed in the deionized water and washed in excess deionized water 10 times to remove the soluble impurities in the hydrogel.

Characterization of hydrogel and composites

Fourier transform infrared spectroscopy (FT-IR)

FT-IR spectrometric (Shimadzu 8400S, Japan) analysis was used to characterize the chemical structure of P (AA-MA) hydrogel and GO/P (AA-MA) composite**.** All samples were prepared as KBr Pellets and spectra in the frequency range (4000-400) cm^{-1}.

Field-Emission Scanning electron microscopy (FE-SEM)

The surface morphology of the composite and hydrogel were examined using Field-Emission scanning electron microscopy (FE-SEM) (Tescan MIRA3, Germany). Analysis of the GO/P(AA-MA) composites and P(AA-MA) hydrogel. The composite and hydrogel were coated with a thin layer of gold under reduced pressure and their FE-SEM images were taken.

Preparation Surface of composite

The surface of the composite in powder forms was washed with excessive amounts of distilled water; several washings were performed to remove dust and soluble materials. The washed surface has then dried an oven at 40 ^{o}C for a period of 6 hours and kept in airtight containers. The surface was then ground and sieved by using different mesh sieve (100-400) μ m. The particle size of 100 μm was used for the surface in all experiments of this work.

Determination of Maximum Absorption (λ_{max})

To determine the maximum wavelength of the CV dye, the ultraviolet-visible absorption spectra of the dye solution (20 mg/L) was recorded within wavelengths of 200-800 nm. The maximum wavelength of the dye solution was determined from its highest absorption in the UV-Vis spectrum found at the wavelength λmax CV = 591.0 nm in Figure (1).

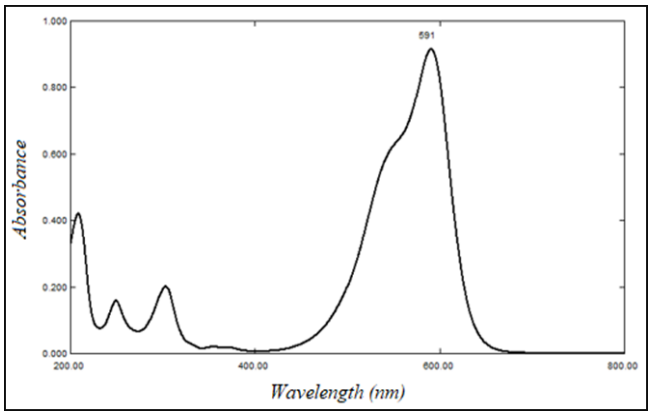

Figure 1: UV-Visible absorption spectra

Calibration Curves of CV dye

Solutions of different concentrations of CV dye prepared by serial dilutions. Absorbance values of these solutions were measured at the selected λmax (591.0 nm) value for dye and plotted against the concentration values CV in Figure (2). The calibration curves in the concentration range that falls in the region of applicability of Beer-Lambert's law were employed.

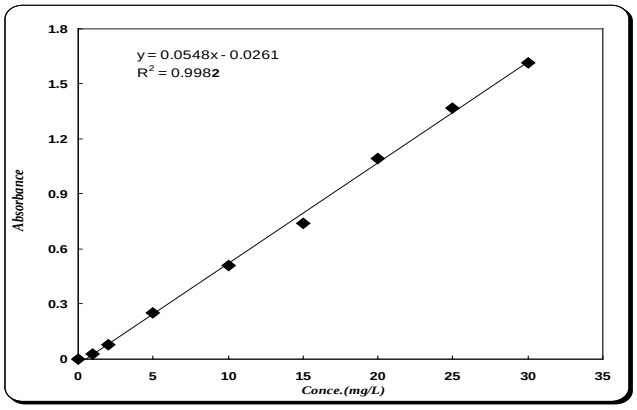

Figure 2: Calibration curves of the CV dye

Determination of the Optimum Amount of graphene oxide in the composite

The different weight ratio of the GO (3-6) mg has been prepared in the composite. Then, added a constant weight of 0.05 g of each ratio to a volume of 10 mL of the CV dye solution at 25 ^{o}C put all the solutions in the shaker and start stirring for 120 min. The end is the separation of the solutions by the centrifuge at 6000 rpm for 15 min and measurement of absorbance after adsorption using a UV-Visible spectrophotometer.

Adsorption Isotherm

The adsorption isotherms were determined by shaking 0.03g of GO/P (AA-MA) composites into 10ml dye solutions, having concentrations ranging from (100-1000) ppm at pH≈7.0. After 120 min. of shaking, the suspensions were centrifuged at 6000 rpm for 10 min. The dye concentration was determined spectrophotometrically. The quantity of CV adsorbed was calculated according to the following equation [22]:-

$$Q_e \text{ or } \frac{x}{m} = \frac{V(C_o - C_e)}{m} \qquad \ldots\ldots(1)$$

Where:

x : the quantity adsorbed.

m : weight of adsorbent (g).

C_o : initial concentration (mg/L).

C_e : equilibrium concentration (mg/ L).

V : volume of solution (L).

Effect of Contact Time

Adsorption kinetic study was carried out by adding known amount (0.03g) of GO/P(AA-MA) composites into 10ml dye solutions (500 ppm). The solutions were centrifuged at a desired time intervals and the residual dye concentration was determined.

Effect of Temperature

Adsorption experiment was repeated in the same manner at temperatures of 15, 20, 25, 30 and 35^{0}C to estimate the basic thermodynamic functions.

Effect of Ionic Strength

The effect of (0.001-0.35 g) sodium chloride, potassium chloride and calcium carbonate solutions containing 500 ppm concentration of CV in electrolyte solution were added to flasks containing (0.03g) of GO/P(AA-MA) composites. The procedure described for the adsorption experiment was followed.

Effect of pH

Adsorption experiment was carried out as mentioned previously as a function of pH using a fixed concentration of CV. Buffer solutions were used to adjust the pH range from 1.0 to 10.0. The pH of the suspensions at the commencement of the adsorption was measured as well as at the end of experiment using pH-meter.

RESULTS AND DISCUSSION

Characterization of graphene oxide

The FTIR spectrum in figure (3) of pristine graphite exhibits no characteristic peak for the discernible functional groups. It only displays four peaks at approximately 1605, 3444, 3010 and 1100 cm^{-1} attributed to the skeletal vibrations from graphite domains (the sp2 aromatic C=C) and the vibration of adsorbed water molecules (the O-H stretching), and correspond to the presence of a C-H and C-H bending bond respectively. After treating with oxidizing agents, the oxygenated graphene sheet could display a series of different absorption bands or characteristics peaks ranging from 900 to 3500 cm^{-1}. The O-H stretching vibration at 3400 cm^{-1} (hydroxyl), the C=O (carboxyl and carbonyl) stretching vibration at 1720 cm^{-1}, the residual sp2 skeletal vibration of un-oxidized graphitic fields (C=C) at 1620 cm^{-1}, the C-O (carboxyl, C-OH) stretching vibration at 1220 cm^{-1}, the C-O (epoxy) groups stretching vibration at 1226 cm^{-1}, the C-O (ring) stretching vibration at 1060 cm^{-1} and C-H stretching at 2950 cm^{-1} [23-25].

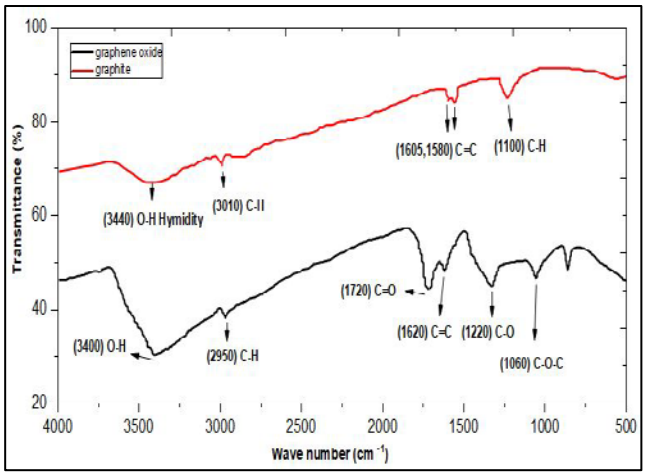

Figure (3: FTIR spectra of Graphite and Graphene Oxide

The FTIR spectra of the P (AA-MA) hydrogel the presence ν(O-H, N-H) overlapping of bonds at (3000-3440) cm^{-1} and C-H stretching at 2890 cm^{-1} and C=O stretching vibration absorption bonds in carboxylic groups at 1720 cm^{-1} but C=O stretching vibration absorption bonds in amide groups at 1650 cm^{-1}, O-H bending for –COOH at 1400 cm^{-1}, and C-O bending at 1560 cm^{-1} ,[26] but the FTIR for GO/P(AA-MA) showed the shift of the groups bands reveals the interactions between the carboxylic groups on P(AA-MA) and GO platelets [27] given in Figure (4).

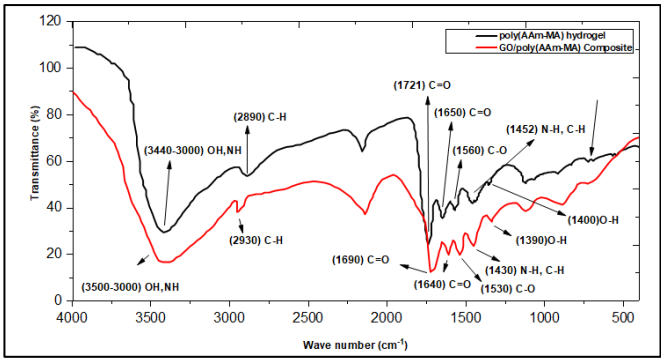

Figure 4: FTIR spectra of P (AA-MA) and GO/P (AA-MA)

FE-SEM a common technique used to identify the surface morphology of graphite, GO, P (AA-MA) and GO/P(AA-MA).FE-SEM image of graphite sheets explain a closely aligned layered structure and be stack as layer thick. It also exhibits flaky appearance for the strong sp^2 carbon-to-carbon bonding in the plane. After oxidation, FE-SEM image of GO nanosheets indicate wavy frizzy appearance, the surface are bristly and the edges of the sheets are foggy. At higher concentration, the surface of GO shows coarse carpet which can due to the link of residual water molecules, carboxyl and hydroxyl groups with the sheets [28, 29] given in Figure (5) and (6).

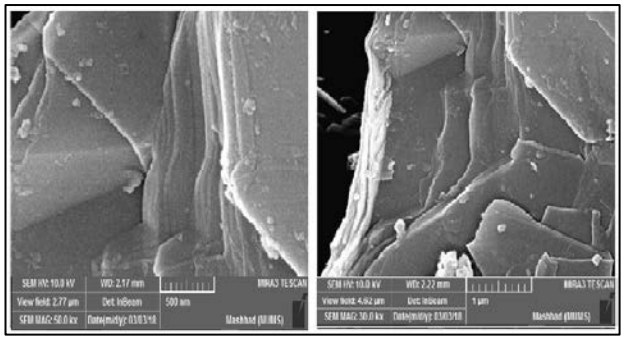

Figure 5: FE-SEM images of Graphite

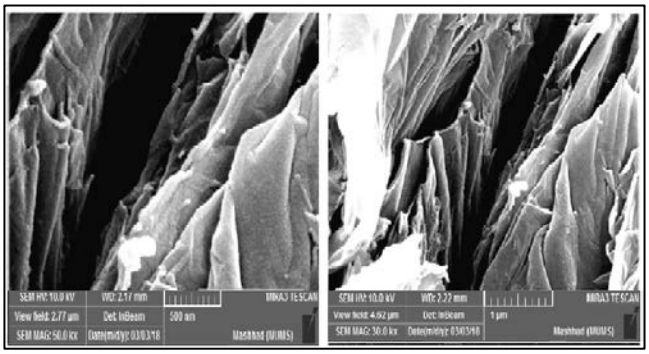

Figure 6: FE-SEM images of GO

The FE-SEM images of P (AA-MA) hydrogel and GO/P (AA-MA) composite samples are shown in Figure (7) and (8) The P (AA-MA) hydrogel shows a smooth and neat surface morphology, and after the introduction of GO platelets into the P (AA-MA) hydrogel network, the surface morphology of the GO/P (AA-MA) composite sample becomes more rough and the GO/P (AA-MA) composite sample shows an irregular, plat-like structure [30]. A plate-like layer of GO platelets may induce the formation of such structure of GO/P (AA-MA). In addition, it can be seen that the GO platelets are well dispersed throughout the polymer matrix as individual platelets and no obvious aggregation was observed. Such a good dispersion of GO platelets into the polymer matrix has also been achieved in other polar polymer GO systems [31].

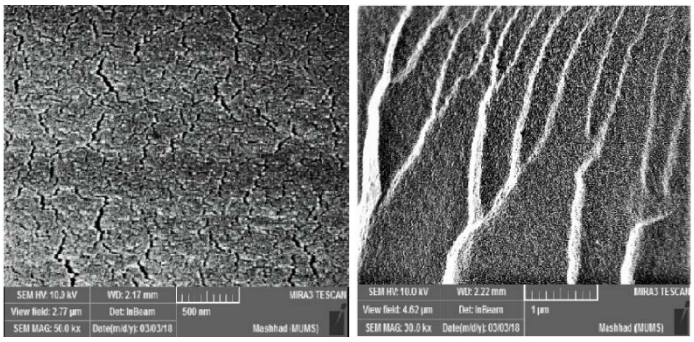

Figure 7: FE-SEM images of P (AA-MA) hydrogel

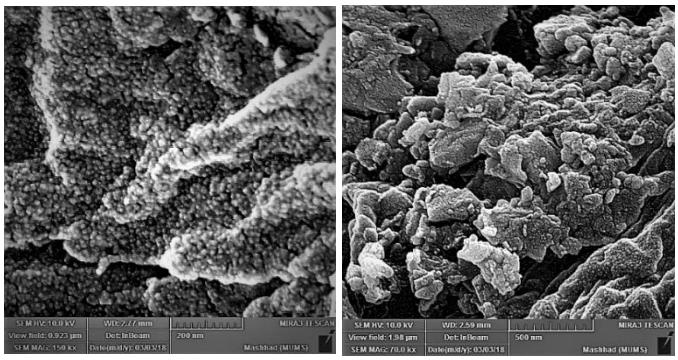

Figure 8: FE-SEM images of GO/P (AA-MA) composite

Adsorption Isotherm

The adsorption of CV from aqueous solution on GO/P (AA-MA) composite has been studied at temperature (25˚C) and at other temperatures (15,20,30 and 35˚C) at pH ≈7.0, where the quantities adsorbed on composite are plotted as a function of equilibrium concentration at the constant temperature. The results showed an increase in adsorptive capacities of composite as the concentration of crystal violet increased (figure 9) because higher dye concentrations provide greater driving force to overcome the mass transfer resistance of dye molecules from aqueous phase to solid phase [32]. However, the rate of increasing in adsorption capacity decreases and finally reaches to a constant value. Composite was found of reasonable surface activity in adsorption from solution of some materials and dyes [33]. CV is the cationic dyes contain functional groups $=N^{+}(CH_3)_2$ in their chemical structure, but the GO / P (AA-MA) surface, it contains negatively charged functional groups such as -COOH, OH, COC, C = O, which in turn will act as hydrogen bonding with dye as well as electrostatic interactions between positive and negative charges for both surface and interference as well as π-π Vandervals forces and thus increasing adsorption.

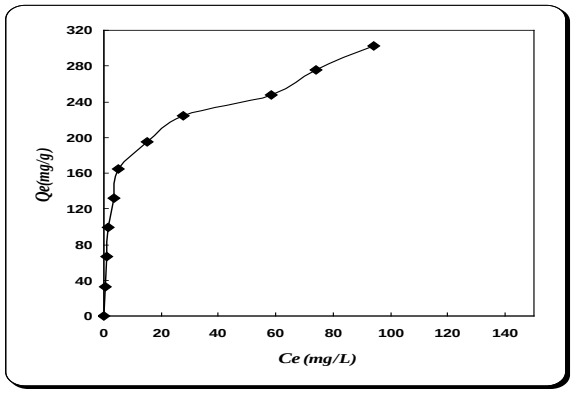

Figure 9: Adsorption isotherm of CV on composite at pH ≈ 7.0 and constant temperature (25 °C)

Langmuir and Freundlich models are two common isotherm models that are widely used to describe adsorption isotherms. In Langmuir isotherm, expressed by equation (2), adsorption occurs as monolayer coverage of adsorbate on homogeneous energetically equivalent adsorbent surface [34, 35].

$$\frac{1}{q_e} = \frac{1}{C_e K_L q_m} + \frac{1}{q_m} \quad \text{…….. (2)}$$

Where C_e is dye equilibrium concentration ($mg.g^{-1}$), K_L is Langmuir adsorption constant related to the energy of adsorption ($L.mg^{-1}$), q_m is maximum adsorption capacity ($mg.g^{-1}$). Freundlich isotherm model considers adsorption as multilayer coverage of adsorbate on heterogeneous adsorbent surface and is expressed as follows:

$$\log q_e = \log K_F + \frac{1}{n}\log C_e \quad \text{…….. (3)}$$

Where C_e is dye equilibrium concentration ($mg.L^{-1}$), K_F is Freundlich constant ($L.g^{-1}$) and n is heterogeneity factor [36]. The plot of Langmuir and Freundlich isotherm models are shown in Figure (10), (11) and the parameters related to each model are listed in table 1. Coefficient factor (R^2) for Langmuir and Freundlich isotherm models is 0.987 and 0.768, respectively, indicating adsorption of CV on the prepared adsorbent is best fitted to the Langmuir isotherm model. According to this model, a high maximum adsorption capacity (qm) up to 84.74 mg g^{-1} was obtained for the prepared adsorbents.

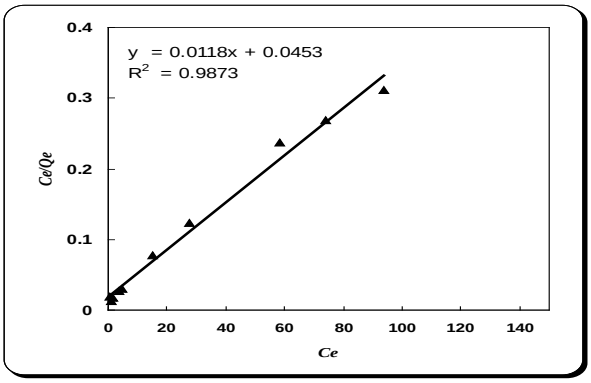

Figure 10: The linearized Langmuir isotherm for CV adsorption at 25^{0}C

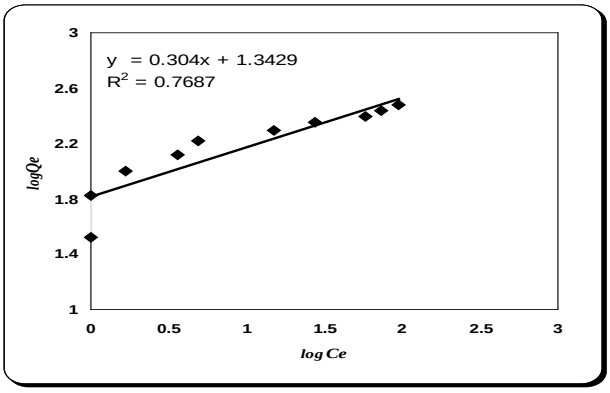

Figure 11: The linearized Freundlich isotherm for CV adsorption at 25^{0}C

Table 1: Isotherm parameters for Langmuir and Freundlich models

Langmuir equation			Freundlich equation		
K_L	q_m	R^2	K_F	n	R^2
0.260	84.745	0.987	22.024	3.289	0.768

Effect of Contact Time

Contact time is an important parameter to determine the efficiency of an adsorbent as a rapid rate of adsorption indicates an efficient adsorbent. In order to determine the effect of contact time on the percentage removal of dyes, adsorption was monitored at particular intervals of time ranging from 1 to 280 min with an initial concentration of 500 ppm , pH 7, and 25^{0}C using an adsorbent dosage of 0.03 g . Figure (12) illustrates the effect of contact time on adsorption capacity of CV. As is apparent from the figure, the initial adsorption stage is rapid for adsorbent, which is due to the adsorption of the molecules on the external surface of the particles. The following stage is a slow adsorption process that the dye molecules slowly diffuse into the porous structure of the adsorbent because many of the available external sites have been occupied at initial stage [37]. It is attributed to adsorption capacity was increased with increasing the time to its maximum value (saturation state) at 120 min.

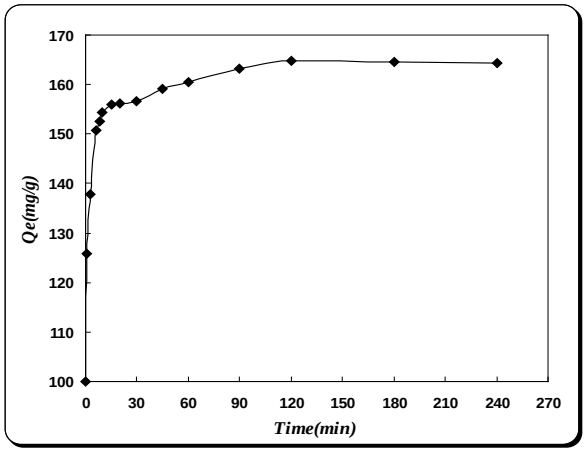

Figure 12: Effect of contact time on CV adsorbed by GO/P (AA-MA) composite

Effect of Temperature and Calculation of Thermodynamic Parameters

The study of adsorption of CV dye on the surface of the GO / p (AA-MA) at a different temperature (15,20,25,30,35) showed that the adsorption process increases with increasing temperature, i.e., the adsorption process is endothermic as shown in Figure (13). This is due to the increasing the temperature cause to an increase in the movement of the dye molecules and an increase in kinetic energy, due to the temperature that increases the rate of diffusion of dye molecules on the surface of the composite resulting in a decrease in the viscosity of the dye solution, Temperature affects the surface of the composite due to the increase in porosity of the surface as well as the increase in pore size [38].

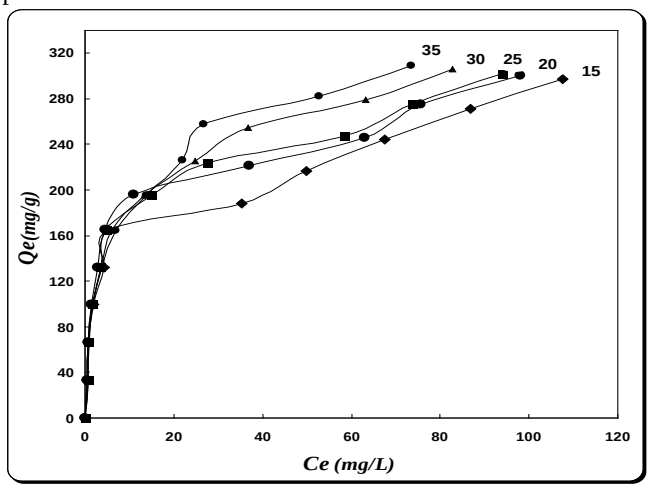

Figure 13: Effect of temperature on the adsorption capacity of dye

Thermodynamic parameters such as standard free energy change (ΔG◦), standard enthalpy change (ΔH◦) and standard entropy change (ΔS◦) were estimated through calculating Xm values at different temperatures [39]. The Gibbs free energy change of adsorption process was calculated by using the following equations:

$\Delta G = - RT \ln K$ ……. (4)

Where K is the dependency of the equilibrium association constant (K = b, from Langmuir constant). T is the solution temperature. The heat of adsorption (ΔH) may be obtained from Van't Hoff equation:

$$\ln X_m = \frac{-\Delta H}{RT} + cons\tan t \quad \text{……. (5)}$$

Entropy change values of adsorption can be calculated from Gibbs equation [40]:

$$\Delta G = \Delta H - T.\Delta S \quad \text{…….. (6)}$$

Table (2) and Figure (14) demonstrate these calculations. The negative of Δ*G* values at given temperatures indicates the spontaneous nature of the adsorption and confirm the feasibility of the adsorption process. Generally, the change in adsorption enthalpy for physical adsorption is in the range of −20 to −40 kJ/mol, but chemisorption is between −400 and −80 kJ/mol [41]. The enthalpy change values were obtained 10.523 kJ/mol for CV. The positive value of Δ*H*◦ reveals the adsorption is endothermic and physical in nature. The enthalpy change value 10.523 kJ/mol indicates the uptake of CV dye on composite to be a physical adsorption. The entropy change values were obtained 63.256 J/ (mol K) for CV. Positive ΔS◦ values of CV adsorption process indicates an irregular increase of the randomness at the solution interface during adsorption.

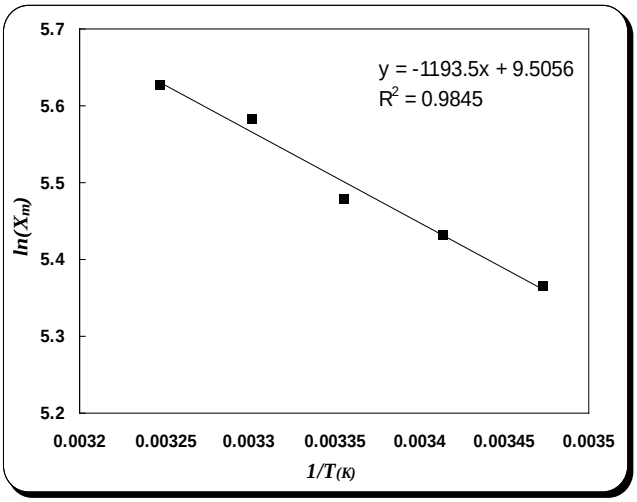

Figure 14: Plot of ln Xm against reciprocal absolute temperature for adsorption crystal violet on composite surface

Table 2: Thermodynamic parameters of adsorption CV on composite surface

ΔH (kJ.mol^{-1})	ΔG (kJ.mol^{-1})	ΔS (J.mol^{-1}.k^{-1})	Equilibrium Constant (K)
10.523	-8.326	63.256	33.630

Effect of Ionic Strength

Commercial dye waste water generally contains high salts contents, it becomes crucial to study the effect of salt concentration on the percentage removal of CV from aqueous solutions using GO / p (AA-MA) composites. Figure (15) illustrates the effect of salts (NaCl, KCl and CaCO3) with variable weight ranging from 0.001 to 0.35 g on CV adsorption capacity by GO / p (AA-MA) composites. From Figure (3-13), it was observed that as the ionic concentration of salts increases, the percentage of adsorption decreases. The size of K^+ and $Ca^{2+}$is greater than that of Na^+ therefore the decrease in adsorption percentage is greater while using KCl and $CaCO_3$. Smaller ions occupy the vacant sites easily. Ca^{2+} has high positive charge than that of Na^+. Therefore, it can mask two negative sites present on the surface of the adsorbent [42]. The decrease in adsorption percentage may be due to the electrostatic interaction between GO / p (AA-MA) composites and the CV molecules are less. According to McBride theory of diffuse double layer model, the ions that form outer-sphere surface complexes the adsorption decreases with increase in ionic strength. Ions that form inner-sphere complexes shows increase in adsorption with increase in ionic strength [[43]. It was found that GO / p (AA-MA) composites forms

outer-sphere complexes with ions. Therefore, adsorption capacity decreases with increase in ionic strength.

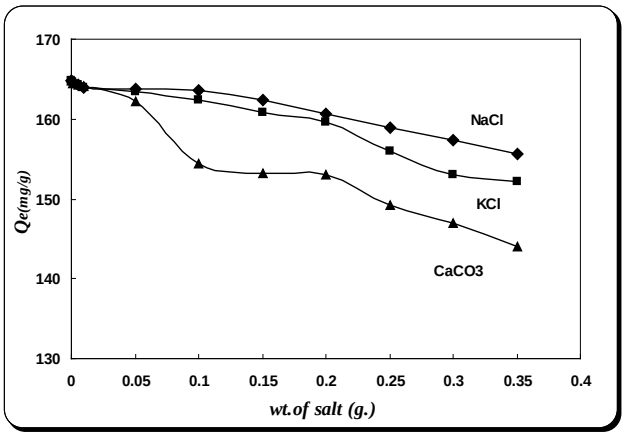

Figure 15: Effect of ionic strength on CV adsorption on the GO / p (AA-MA) composite

Effect of pH

Since pH of the solution has a strong effect on dye adsorption, experiments were conducted in solutions with different pH adjusted by the addition of HCl or NaOH solutions (0.01 N). Adsorption of MB in solutions with pH range from 1 to 10 was investigated and the results are shown in Figure (16). There are many functional groups such as hydroxyl and carboxyl groups in the structure of the prepared adsorbent. In neutral or basic pH values, adsorption capacity is very high due to strong electrostatic interactions between adsorbent and dye molecules. However by decreasing pH to acidic ranges, functional groups of adsorbent become protonated which leads to a repulsion between adsorbent and positively charged dye molecules. Therefore, adsorption capacity decreases in lower pH values.

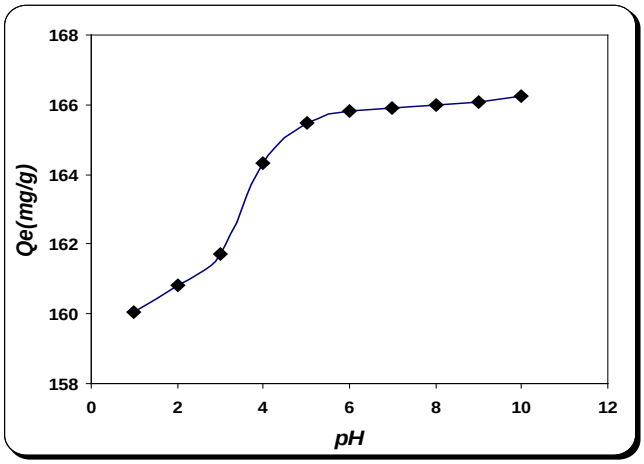

Figure 16: Effect of solution pH values on CV adsorption on the GO / p (AA-MA) composite

CONCLUSIONS

(GO) /poly (acrylic acid – maleic acid) superabsorbent composites were used as an adsorbent to remove conventional cationic dyes (Crystal Violet) from aqueous solutions. Contact time, ionic strength, initial concentration, and temperature and solution pH played considerable role on the adsorption capacity of composites hydrogel. Langmuir isotherm equation model showed that it could describe the adsorption of CV on the composite hydrogel better than Freundlich model. Negative values of the free energy change, ΔG°, showed that CV adsorption by composites hydrogel was spontaneous. Positive values in enthalpy change ΔH° represent that the adsorption mechanism is found to be endothermic.

REFERENSES

(1) Robinson, T.; McMullan, G.; Marchant, R.; Nigam, P. Remediation of dyes in textile effluent: a critical review on current treatment technologies with a proposed alternative. *Bioresource technology*, 2001, 77(3): 247-255.

(2) O'Neill, C.; Hawkes, F.R.; Hawkes, D.L.; Lourenço, N.D.; Pinheiro, H.M.; Delée, W. Colour in textile effluents–sources, measurement, discharge consents and simulation: a review. *Journal of Chemical Technology & Biotechnology: International Research in Process, Environmental & Clean Technology*, 1999, 74(11): 1009-1018.

(3) Sulak, M.; Demirbas, E.; Kobya, M. Removal of Astrazon Yellow 7GL from aqueous solutions by adsorption onto wheat bran. *Bioresource technology*, 2007, 98(13): 2590-2598.

(4) Li, H.; Wan, J.; Ma, Y.; Wang, Y.; Huang, M. Influence of particle size of zero-valent iron and dissolved silica on the reactivity of activated persulfate for degradation of acid orange 7. *Chemical Engineering Journal*, 2014, 237: 487-496.

(5) Anjaneyulu, Y.; Chary, N.S.; Raj, D.S.S. Decolourization of industrial effluents–available methods and emerging technologies–a review. *Reviews in Environmental Science and Bio/Technology*, 2005, 4(4): 245-273.

(6) Nassar, M.M.; El-Geundi, M.S. Comparative cost of colour removal from textile effluents using natural adsorbents. *Journal of Chemical Technology & Biotechnology*, 1991, 50(2): 257-264.

(7) Copello, G.J.; Mebert, A.M.; Raineri, M.; Pesenti, M.P.; Diaz, L.E. Removal of dyes from water using chitosan hydrogel/SiO2 and chitin hydrogel/SiO2 hybrid materials obtained by the sol–gel method. *Journal of hazardous materials*, 2011, 186(1): 932-939.

(8) Crini, G. Non-conventional low-cost adsorbents for dye removal: a review. *Bioresource technology*, 2006, 97(9): 1061-1085.

(9) Wang, A.; Cui, Y.; Li, J.; van Hest, J.C. Fabrication of gelatin microgels by a "cast" strategy for controlled drug release. *Advanced Functional Materials*, 2012, 22(13): 2673-2681.

(10) Zou, Q.; Zhang, L.; Yan, X.; Wang, A.; Ma, G.; Li, J.; Möhwald, H.; Mann, S. Multifunctional Porous Microspheres Based on Peptide–Porphyrin Hierarchical Co-Assembly. *Angewandte Chemie*, 2014, 126(9): 2398-2402.

(11) Du, M.; Song, W.; Cui, Y.; Yang, Y.; Li, J. Fabrication and biological application of nano-hydroxyapatite (nHA)/alginate (ALG) hydrogel as scaffolds. *Journal of Materials Chemistry*, 2011, 21(7): 2228-2236.

(12) Zhu, P.; Yan, X.; Su, Y.; Yang, Y.; Li, J. Solvent-Induced Structural Transition of Self-Assembled Dipeptide: From Organogels to Microcrystals. *Chemistry–A European Journal*, 2010, 16(10): 3176-3183.

(13) Yan, X.; Cui, Y.; He, Q.; Wang, K.; Li, J. Organogels based on self-assembly of diphenylalanine peptide and their application to immobilize quantum dots. *Chemistry of Materials*, 2008, 20(4): 1522-1526.

(14) Matson, J.B.; Newcomb, C.J.; Bitton, R.; Stupp, S.I. Nanostructure-templated control of drug release from peptide amphiphile nanofiber gels. *Soft Matter*, 2012, 8(13): 3586-3595.

(15) Mateen, R.; Hoare, T. Injectable, in situ gelling, cyclodextrin–dextran hydrogels for the partitioning-driven release of hydrophobic drugs. *Journal of Materials Chemistry B*, 2014, 2(32): 5157-5167.

(16) Moysan, E.; González-Fernández, Y.; Lautram, N.; Béjaud, J.; Bastiat, G.; Benoit, J.-P. An innovative hydrogel of gemcitabine-loaded lipid nanocapsules: when the drug is a key player of the nanomedicine structure. *Soft matter*, 2014, 10(11): 1767-1777.

(17) Rodrigues, M.; Calpena, A.C.; Amabilino, D.B.; Garduño-Ramírez, M.L.; Pérez-García, L. Supramolecular gels based on a gemini

imidazolium amphiphile as molecular material for drug delivery. *Journal of Materials Chemistry B*, 2014, 2(33): 5419-5429.
(18) Azarang, M.; Shuhaimi, A.; Sookhakian, M. Crystalline quality assessment, photocurrent response and optical properties of reduced graphene oxide uniformly decorated zinc oxide nanoparticles based on the graphene oxide concentration. *RSC Advances*, 2015, 5(65): 53117-53128.
(19) Pham, V.H.; Gebre, T.; Dickerson, J.H. Facile electrodeposition of reduced graphene oxide hydrogels for high-performance supercapacitors. *Nanoscale*, 2015, 7(14): 5947-5950.
(20) Huang, H.; Lü, S.; Zhang, X.; Shao, Z. Glucono-δ-lactone controlled assembly of graphene oxide hydrogels with selectively reversible gel–sol transition. *Soft Matter*, 2012, 8(17): 4609-4615.
(21) Marcano, D.C.; Kosynkin, D.V.; Berlin, J.M.; Sinitskii, A.; Sun, Z.; Slesarev, A.; Alemany, L.B.; Lu, W.; Tour, J.M. Improved synthesis of graphene oxide. *ACS nano*, 2010, 4(8): 4806-4814.
(22) Atkins, P.; De Paula, J.; Keeler, J. *Atkins' physical chemistry*;Oxford university press. 2018.
(23) Chua, C.K.; Ambrosi, A.; Pumera, M. Graphene oxide reduction by standard industrial reducing agent: thiourea dioxide. *Journal of materials chemistry*, 2012, 22(22): 11054-11061.
(24) Zhang, X.; Li, K.; Li, H.; Lu, J.; Fu, Q.; Chu, Y. Graphene nanosheets synthesis via chemical reduction of graphene oxide using sodium acetate trihydrate solution. *Synthetic Metals*, 2014, 193: 132-138.
(25) Alwan, S.H.; Alshamsi, H.A.H.; Jasim, L.S. Rhodamine B removal on A-rGO/cobalt oxide nanoparticles composite by adsorption from contaminated water. *Journal of Molecular Structure*, 2018, 1161: 356-365.
(26) Radhy, N.D. Naproxen Sodium Release from Poly (acrylic acid-co-N-vinyl-2-pyrrolidone) Hydrogels. *Al-Qadisiyah Journal Of Pure Science*, 2017, 21(3).
(27) Lee, S.; Lee, H.; Sim, J.H.; Sohn, D. Graphene oxide/poly (acrylic acid) hydrogel by γ-ray pre-irradiation on graphene oxide surface. *Macromolecular Research*, 2014, 22(2): 165-172.
(28) He, H.; Gao, C. General approach to individually dispersed, highly soluble, and conductive graphene nanosheets functionalized by nitrene chemistry. *Chemistry of Materials*, 2010, 22(17): 5054-5064.
(29) Aunkor, M.; Mahbubul, I.; Saidur, R.; Metselaar, H. Deoxygenation of graphene oxide using household baking soda as a reducing agent: a green approach. *RSC Advances*, 2015, 5(86): 70461-70472.
(30) Jiang, Z.; Li, Q.; Chen, M.; Li, J.; Li, J.; Huang, Y.; Besenbacher, F.; Dong, M. Mechanical reinforcement fibers produced by gel-spinning of poly-acrylic acid (PAA) and graphene oxide (GO) composites. *Nanoscale*, 2013, 5(14): 6265-6269.
(31) Wan, S.; Hu, H.; Peng, J.; Li, Y.; Fan, Y.; Jiang, L.; Cheng, Q. Nacre-inspired integrated strong and tough reduced graphene oxide–poly (acrylic acid) nanocomposites. *Nanoscale*, 2016, 8(10): 5649-5656.
(32) Tanhaei, B.; Ayati, A.; Lahtinen, M.; Sillanpää, M. Preparation and characterization of a novel chitosan/Al2O3/magnetite nanoparticles composite adsorbent for kinetic, thermodynamic and isotherm studies of Methyl Orange adsorption. *Chemical engineering journal*, 2015, 259: 1-10.
(33) Bradshaw, A. G. Wedler: Chemisorption: An Experimental Approach Butterworths, London. Boston 1976. 250 Seiten, Prets:£ 12.-(Übersetzt von DF Klemperer). *Berichte der Bunsengesellschaft für physikalische Chemie*, 1977, 81(7): 705-705.
(34) Trade, H.A.; Jassim, L.S.; Al-Taweel, S.S.J. A study of adsorption of crystal violet from aqueous solution on kaolin. *Iraqi National Journal Of Chemistry*, 2007, (28): 642-654.
(35) Al-Taweel, S.S.J.; Jassim, L.S.; Khlwy, F.S. A study of Adsorption of Crystal Violet from Aqueous Solution on Polyester. *journal of al-qadisiyah for pure science (quarterly)*, 2007, 12(4): 120-129.
(36) Yagub, M.T.; Sen, T.K.; Afroze, S.; Ang, H.M. Dye and its removal from aqueous solution by adsorption: a review. *Advances in colloid and interface science*, 2014, 209: 172-184.
(37) Mittal, A.; Mittal, J.; Malviya, A.; Kaur, D.; Gupta, V. Adsorption of hazardous dye crystal violet from wastewater by waste materials. *Journal of Colloid and Interface Science*, 2010, 343(2): 463-473.
(38) Mahdavinia, G.R.; Massoudi, A.; Baghban, A.; Shokri, E. Study of adsorption of cationic dye on magnetic kappa-carrageenan/PVA nanocomposite hydrogels. *Journal of Environmental Chemical Engineering*, 2014, 2(3): 1578-1587.
(39) Jaism, L.; Radhy, N.; Kmal, R. A study of Adsorption of Azure B and C from Aqueous Solutions on Poly (Acryl amide-co-Crotonic acid) Hydro gels Surface. *Chem. and Pro. Eng. Research*, 2015, 32: 62-69.
(40) Zhang, L.; Zhang, H.; Guo, W.; Tian, Y. Removal of malachite green and crystal violet cationic dyes from aqueous solution using activated sintering process red mud. *Applied Clay Science*, 2014, 93: 85-93.
(41) Mittal, A.; Gajbe, V.; Mittal, J. Removal and recovery of hazardous triphenylmethane dye, Methyl Violet through adsorption over granulated waste materials. *Journal of Hazardous Materials*, 2008, 150(2): 364-375.
(42) Anirudhan, T.S.; Divya, P.L.; Nima, J.; Sandeep, S. Synthesis and evaluation of Iron-doped titania/silane based hydrogel for the adsorptional photocatalytic degradation of Victoria blue under visible light. *Journal of colloid and interface science*, 2014, 434: 48-58.
(43) McBride, M.B. A critique of diffuse double layer models applied to colloid and surface chemistry. *Clays and Clay minerals*, 1997, 45(4): 598-608.